J. Membrane Biol. 154, 53–67 (1996)

The Journal of
Membrane
Biology

A Mathematical Model of the Pancreatic Ductal Epithelium

Y. Sohma[1,*], M.A. Gray[1], Y. Imai[2], B.E. Argent[1]

[1]Department of Physiological Sciences, University Medical School, Framlington Place, Newcastle upon Tyne NE2 4HH, UK
[2]Department of Physiology, Osaka Medical College, Takatsuki Osaka 569, Japan

Received: 18 October 1995/Revised: 5 July 1996

Abstract. A mathematical model of the HCO_3^--secreting pancreatic ductal epithelium was developed using network thermodynamics. With a minimal set of assumptions, the model accurately reproduced the experimentally measured membrane potentials, voltage divider ratio, transepithelial resistance and short-circuit current of nonstimulated ducts that were microperfused and bathed with a CO_2/HCO_3^--free, HEPES-buffered solution, and also the intracellular pH of duct cells bathed in a CO_2/HCO_3^--buffered solution. The model also accurately simulated: (i) the effect of step changes in basolateral K^+ concentration, and the effect of K^+ channel blockers on basolateral membrane potential; (ii) the intracellular acidification caused by a Na^+-free extracellular solution and the effect of amiloride on this acidification; and (iii) the intracellular alkalinization caused by a Cl^--free extracellular solution and the effect of DIDS on this alkalinization. In addition, the model predicted that the luminal Cl^- conductance plays a key role in controlling both the HCO_3^- secretory rate and intracellular pH during HCO_3^- secretion. We believe that the model will be helpful in the analysis of experimental data and improve our understanding of HCO_3^--transporting mechanisms in pancreatic duct cells.

Key words: Pancreatic duct — Mathematical model — HCO_3^- secretion — Intracellular pH regulation — Cystic fibrosis transmembrane conductance regulator

Introduction

The ductal epithelial cells of the pancreas form a network of branching tubules whose function is to convey digestive enzymes (secreted by the acinar cells) into the intestine [3, 5]. However, the ducts are not merely passive conduits but also secrete an alkaline fluid, rich in $NaHCO_3$, which washes the digestive enzymes down the ductal tree and also partially neutralizes acid chyme entering the duodenum from the stomach. The maximum concentration of HCO_3^- found in pancreatic juice depends on the species, and varies between about 70 mM in the rat and 145 mM in cat, dog and humans [3, 5].

The ductal tree forms only a small proportion of the pancreatic mass (2 to 14% depending on species, [3]), and this virtually precludes the direct study of duct cell function *in situ.* However, in the 1980s a number of groups developed techniques for the isolation of small interlobular and intralobular pancreatic ducts (which are probably the main site of HCO_3^- secretion [3]), and have used electrophysiological and spectrofluorometric techniques to study the cellular mechanism of HCO_3^- secretion [9, 23, 24, 38]. As a result of these studies, most of which have been performed on ducts isolated from the rat pancreas, the HCO_3^- secretory model shown in Fig. 1 has been proposed [9, 23, 24]. In brief, the initial step in HCO_3^- transport is thought to be diffusion of CO_2 into the duct cell and its hydration to carbonic acid by carbonic anhydrase. The carbonic acid then dissociates into H^+ and HCO_3^- ions and the proton is translocated back across the basolateral membrane on a Na^+/H^+ exchanger. Effectively, this is the active transport step for HCO_3^-, with the energy being provided by the Na^+ gradient established by the Na^+/K^+ ATPase. Once accumulated inside the duct cell, the HCO_3^- ion is then secreted across the apical membrane on a Cl^-/HCO_3^- exchanger. The rate at which these exchangers cycle is thought to be controlled by the opening of Cl^- channels on the apical plasma membrane. To date, cyclic AMP-activated, cystic fibrosis transmembrane conductance regulator (CFTR) Cl^- channels, and Ca^{2+}-activated Cl^- channels have been identified on the apical plasma membrane of the duct

Correspondence to: B.E. Argent

* *Present address:* Department of Physiology, Osaka Medical College, Takatsuki Osaka 569, Japan

cell. These ion channels are key regulatory points in the HCO_3^- secretory mechanism and can be viewed as having two roles: (i) to provide luminal Cl^- for operation of the apical anion exchanger, and (ii) to dissipate the intracellular chloride that accumulates as the anion exchangers cycle. At the moment the model is based solely on the localization of transport elements in the duct cell, and the way in which they respond when HCO_3^- secretion is stimulated. Experimental validation of the model will require the measurement of the electrochemical gradients for the transported ions across the apical and basolateral membranes of the duct cell.

Previously, mathematical models have been employed to analyze ion transport events in a number of epithelia (frog skin: [16, 20, 22], renal tubule: [7, 41, 43], airway epithelium: [13], secretory epithelia: [6]), including the exocrine pancreas [19]. Our aim in this study was to develop a mathematical version of the duct cell model described above, and to test whether it would predict the behavior of the duct cell in both the transient and steady states. In this paper we mainly confine ourselves to a description of the model and to a comparison of its behavior with published experimental data. However, we have also asked whether the basic model will work—i.e., will it secrete HCO_3^- at the concentrations found in pancreatic juice while at the same time maintaining reasonable values for the intracellular and electrical parameters?

Some of our data have been presented in preliminary form [32, 33].

Materials and Methods

List of Symbols

Subscripts

k: Compartment. *l:* luminal, *c:* intracellular, *bl:* basolateral, *b:* bath (in single-cell version).
m: Membrane (pathway). *l:* luminal, *bl:* basolateral, *j:* junctional.
i: Solute. *X:* total of solutes impermeable to membrane.

Compartment Variables

$c^{(k)}_i$, $[i]_{(k)}$: Concentration of solute *i* in a compartment (*k*).
$\mu^{(k)}_i$: Chemical potential of solute *i* in a compartment (*k*).
$\tilde{\mu}^{(k)}_i$: Electrochemical potential of solute *i* in a compartment (*k*).
$p_{(k)}$: Static pressure in a compartment (*k*).
$\pi_{(k)}$: Osmotic pressure in a compartment (*k*).
$Vol_{(k)}$: Volume per 1 cm^2 epithelium of a compartment (*k*).
$E_{(k)}$: Electrical potential of a compartment (*k*).

Compartment Parameters

$C_{p(k)}$: Compliance of a compartment (*k*).
$C_{e(k)}$: Electrical capacitance of a compartment (*k*).

Membrane Parameters

$A_{(m)}$: Area of a membrane (*m*) per 1 cm^2 epithelium, cm^2.
$Lp_{(m)}$: Water permeability of a membrane (*m*).
$w_{i(m)}$: Permeability coefficient of solute *i* in a membrane (*m*).
σ_i: Reflection coefficient of solute *i* in a membrane.
$\bar{c}_i$: Mean concentration of solute *i* in a membrane.
$G_{Na/H}$: Permeability coefficient for Na^+/H^+ antiporter.
$G_{Cl/HCO3}$: Permeability coefficient for Cl^-/HCO_3^- antiporter.
K_i: Dissociation constant for binding of solute *i* to its site on the antiporter.
G_{pump}: Permeability coefficient for Na^+/K^+ pump.
E_{rev}: Reversal potential of pump current.
K_{pi}: Dissociation constant for binding of solute *i* to its site on the Na^+/K^+ pump.

Buffering Parameters

K_{CO2}: Dissociation constant of HCO_3^-/CO_2 buffering system.
K_{HB}: Dissociation constant of intrinsic buffering system.

Fluxes and Flows

J_v: Water flux through a membrane.
$J_{i(m)}$: Total flux of solute *i* through a membrane (*m*).
J_{di}: Flux of solute *i* through diffusion pathway in a membrane.
$J_{Na/H:}$ Turnover rate of the Na^+/H^+ antiporter.
$J_{Cl/HCO3}$: Turnover rate of the Cl^-/HCO_3^- antiporter.
J_{pump}: Turnover rate of the Na^+/K^+ pump.
$Flw_{v(k)}$: Net water influx into a compartment (*k*).
$Flw_{i(k)}$: Net influx of solute *i* into a compartment (*k*).
$Flw_{e(k)}$: Net influx of positive charge into a compartment (*k*).

Constants

dt: Integration intervals.
z_i: Valence of solute *i.*
R: Molar gas constant.
T: Absolute temperature.
F: Faraday's constant.
$\triangle$: Difference.

The Model

Our mathematical model of the pancreatic duct cell comprised the transport elements shown in Fig. 1. There are two different versions of the model. One version simulates an epithelial cell *in situ* within an intact duct (Fig. 1*A*), and the other version an isolated duct cell (Fig. 1*B*). The intact duct version is based on data obtained from microelectrode studies on microperfused ducts [23, 24, 25], while the single-cell version is based on fluorescent dye and patch-clamp studies performed on nonperfused ducts and on single duct cells [8, 9, 10, 11, 37, 38, 40]. The intact duct and single-cell versions are three- and two-compartment models respectively. The sole difference between the two versions of the model is the inclusion of a junctional pathway in the intact duct simulation (Fig. 1*A*). Otherwise, both versions are identical and use a common set of parameters.

Variables

The model variables included intracellular $[Na^+]$, $[K^+]$, $[Cl^-]$, $[HCO_3^-]$ and pH, membrane potential, and cell volume. Cell volume includes

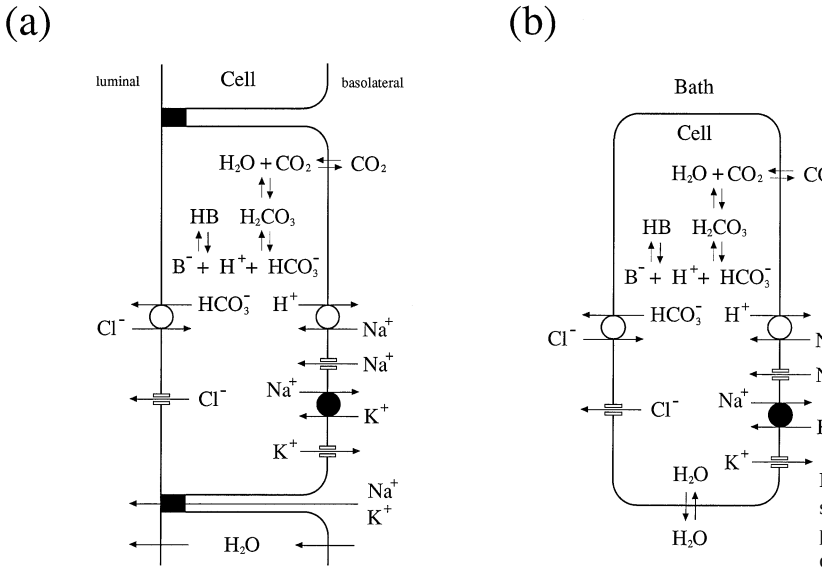

Fig. 1. Schematic representation of the ion transport systems in the mathematical models of: (*A*) an intact pancreatic duct, and (*B*) a single isolated pancreatic duct cell.

fluid and nonfluid components. The nonfluid component was assumed to be 40% of the initial value of the cell volume. Therefore, cell volume (Vol_{cell}), is the form of:

$$Vol_{cell} = Vol_c + 0.4 \cdot Vol_{cell}^{initial} \quad (1)$$

where Vol_c is the volume of the intracellular compartment, which is equal to the volume of water in the cell, and $Vol_{cell}^{initial}$ is the initial cell volume.

Membrane potentials are defined as follows:

$$PD_1 = E_{(c)} - E_{(l)} \quad (2a)$$
$$PD_{bl} = E_{(c)} - E_{(bl)} \quad (2b)$$
$$PD_{te} = E_{(l)} - E_{(bl)} \quad (2c)$$

where PD_1, PD_{bl} and PD_{te} are luminal membrane, basolateral membrane and transepithelial potential differences, respectively.

It was assumed that $[Na^+]$, $[K^+]$, $[Cl^-]$, $[HCO_3^-]$, pH and volumes in the luminal and basolateral compartments remained constant during simulations. This assumption was realized by setting very large initial values for the volumes of both compartments (10^{80} ml/cm^2 epithelium; *see* Table 2).

Model Equations

The mathematical model simulates membrane transport and cellular buffering systems in the duct cell. The membrane transport system in the mathematical model (Fig. 1*A* and *B*) includes the following parameters: cell membrane water permeability, apical Cl^- conductance and Cl^-/HCO_3^- antiporter, basolateral K^+ and Na^+ conductances, Na^+/H^+ antiporter and Na^+/K^+-pump and paracellular nonselective cation conductance. The intracellular buffering system contains intracellular HCO_3^-/CO_2 buffering and intrinsic non-CO_2 buffering systems. It was assumed that all the parameters in the transport and buffering equations remained constant during simulations.

I. Transport Equations

The equations for water and electrolyte transport were derived using network thermodynamics [16, 26], and were as follows:

Table 1. Composition of the bathing solutions used in the computer model

Solution	HEPES-buffered	HCO_3^-/CO_2-buffered
Na^+ (mM)	146	146
K^+ (mM)	5	5
Cl^- (mM)	150	125
HCO_3^- (mM)	0.2	25
X (mM)	14.3	14.5
pH	7.4	7.4
pCO_2 (mmHg)	0.32	40
Osmolarity (mOsm)	315.5	315.5

Table 2. Values of the compartment parameters (C_p and C_e), and the initial compartment volumes ($Vol_{initial}$) used in the model

	Luminal	Intracellular	Basolateral
C_p (l/atm)	1.0×10^{80}	1.0×10^{80}	1.0×10^{80}
C_e (F)	8×10^{-4}	8×10^{-4}	8×10^{-4}
$Vol_{initial}$ (ml/cm^2)	1.0×10^{80}	6.0×10^{-4}	1.0×10^{80}

Water Transport. The volume flux across a membrane is given by:

$$J_v = L_p \left\{ \triangle p - \triangle \pi + \sum_i (1 - \sigma_i) \bar{c}_i \triangle \tilde{\mu}_i \right\} \quad (3a)$$

where L_p is the water permeability, σ_i is the reflection coefficient of solute *i*, $\triangle p$ is the hydrostatic pressure difference, $\triangle \pi$ is the osmotic pressure difference,

$$\triangle \pi = \sum_i RT \triangle c_i \quad (3b)$$

$\triangle \tilde{\mu}_i$ is the electrochemical potential difference of solute *i*,

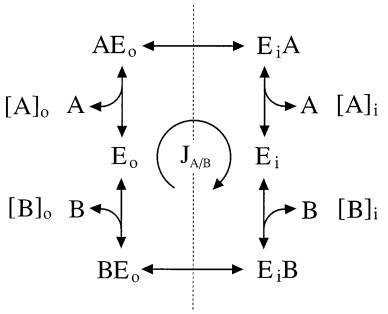

Fig. 2. Kinetic model used to derive the turnover rates of the Na^+/H^+ exchanger ($J_{Na/H}$) and the Cl^-/HCO_3^- antiporter ($J_{Cl/HCO3}$).

$$\triangle\tilde{\mu}_i = RT\triangle \ln c_i + z_iF\triangle E \tag{3c}$$

and $\bar{c}_i$ is a mean membrane solute concentration,

$$\bar{c}_i = \frac{\triangle c_i}{\triangle \ln c_i} \tag{3d}$$

where $\triangle E$ is the electrical potential difference, c_i and z_i are the concentration and the valence of solute *i* respectively. *R*, *T*, *F* and $\triangle$ have their usual meanings.

When $\triangle \ln c_i$ is 0 or close to 0, the following simplified equation was used,

$$\bar{c}_i = \frac{c_i^1 + c_i^2}{2} \tag{3d'}$$

where c_i^1 and c_i^2 are the concentrations of solute *i* in the two compartments separated by the membrane.

Electrolyte Transport. Electrolyte transport in the model occurs through single ion diffusive pathways, antiporters and the Na^+/K^+ pump.

1. Single ion diffusive pathway (*conductance*). Transmembrane flux of solute *i* (J_{di}) through a single ion diffuse pathway is described by the equation:

$$J_{di} = (1 - \sigma_i)\bar{c}_i J_v + w_i\bar{c}_i\triangle\tilde{\mu}_i \tag{4}$$

where w_i is the permeability coefficient of solute *i.* Unless otherwise specified, the model contained a Cl^- diffusive pathway on the apical membrane, Na^+ and K^+ diffusive pathways on the basolateral membrane and, in the intact duct version, Na^+ and K^+ diffusive pathways in the tight junctions (the paracellular pathway).

2. Antiporter. The model has Cl^-/HCO_3^- and Na^+/H^+ antiporters located on the apical and basolateral membranes respectively. Expressions for the turnover rates of these exchangers were derived from the kinetic scheme shown in Fig. 2. We assumed: (i) that these antiporters had a single site which bound the transported ions; (ii) that the transported ions competed for the single binding site; (iii) that the antiporters did not cross the membrane in the absence of a bound ion; (iv) that the velocity constants (*P*) for transport from the outside to inside and *vice versa* were the same; and (v) that the dissociation constants (K_A, K_B) for each ion at the intracellular and extracellular faces of the membrane were the same. Therefore:

$$[A]_o[E_o] = K_A[AE_o] \tag{5a}$$
$$[B]_o[E_o] = K_B[BE_o] \tag{5b}$$
$$[A]_i[E_i] = K_A[E_iA] \tag{5c}$$
$$[B]_i[E_i] = K_B[E_iB] \tag{5d}$$
$$[E_o] + [E_i] + [AE_o] + [BE_o] + [E_iA] + [E_iB] = [E_t] \tag{5e}$$
$$P([AE_o] - [E_iA]) = P([E_iB] - [BE_o]) = J_{A/B} \tag{5f}$$

From equations 5*a*–5*f*,

$$J_{A/B} = \frac{G_{A/B}([A]_o[B]_i - [A]_i[B]_o)}{K_AK_B\{(1 + [A]_i/K_A + [B]_i/K_B)([A]_o/K_A + [B]_o/K_B) + (1 + [A]_o/K_A + [B]_o/K_B)([A]_i/K_A + [B]_i/K_B)\}} \tag{5g}$$

where $G_{A/B} = P[E_t]$.

Therefore, the turnover rates of the Na^+/H^+ exchanger ($J_{Na/H}$), and the Cl^-/HCO_3^- antiporter ($J_{Cl/HCO3}$), can be expressed as follows.

$$J_{Na/H} = \frac{G_{Na/H}([Na^+]_{bl}[H^+]_c - [Na^+]_c[H^+]_{bl})}{K_{Na}K_H\{(1 + [Na^+]_{bl}/K_{Na} + [H^+]_{bl}/K_H)([Na^+]_c/K_{Na} + [H^+]_c/K_H) + (1 + [Na^+]_c/K_{Na} + [H^+]_c/K_H)([Na^+]_{bl}/K_{Na} + [H^+]_{bl}/K_H)\}} \tag{5h}$$

$$J_{Cl/HCO3} = \frac{G_{Cl/HCO3}([Cl^-]_l[HCO_3^-]_c - [Cl^-]_c[HCO_3^-]_l)}{K_{Cl}K_{HCO3}\{(1 + [Cl^-]_c/K_{Cl} + [HCO_3^-]_c/K_{HCO3})([Cl^-]_l/K_{Cl} + [HCO_3^-]_l/K_{HCO3}) + (1 + [Cl^-]_l/K_{Cl} + [HCO_3^-]_l/K_{HCO3})([Cl^-]_c/K_{Cl} + [HCO_3^-]_c/K_{HCO3})\}} \tag{5i}$$

where $G_{Na/H}$ and $G_{Cl/HCO3}$ are the permeability coefficients for the Na^+/H^+ and Cl^-/HCO_3^- antiporters respectively. The dissociation constants (K_{Na} = 100 mM, K_H = 0.5 μM, K_{Cl} = 10 mM and K_{HCO3} = 1 mM) were derived from data in the literature [14, 15, 18, 31, 38, 39, 40].

3. Na^+/K^+ pump. The turnover rate of the Na^+/K^+ pump (J_{pump}), was expressed as previously described by Hartmann & Verkman [13].

$$J_{pump} = G_{pump}([Na^+]_c/[Na^+]_c + K_{pNa})^3([K^+]_{bl}/[K^+]_{bl} + K_{pK})^2 (PD_{bl} - E_{rev}) \tag{6}$$

The saturation constants were K_{pNa} = 25 mM for intracellular Na^+, and K_{pK} = 1.4 mM for extracellular K^+. The turnover rate is assumed to be linearly dependent on the basolateral membrane potential (PD_{bl}) with a reversal potential (E_{rev}) of −200 mV under physiological conditions [1, 29, 46]. One cycle of the Na^+/K^+ pump was assumed to move $2K^+$ into, and $3Na^+$ out of, the cell.

II. Buffering Equations

The model contains an intracellular HCO_3^-/CO_2 buffering system and an intrinsic non-CO_2 buffering system. Intracellular H^+ was buffered by both of these systems.

1. HCO_3^-/CO_2 Buffering System. When H^+ is added to the intracellular compartment, H^+ combines with HCO_3^- according to the reaction,

$$H^+ + HCO_3^- \leftrightarrow CO_2 + H_2O \tag{7}$$

This equilibrium is governed by the law of mass action,

$$[H^+]_c[HCO_3^-]_c = K_{CO2} \cdot pCO_{2c} \tag{8}$$

where K_{CO2} is the apparent acid dissociation constant of the HCO_3^-/CO_2 buffering system. The value of K_{CO2} was set at 24.9 pM/mmHg.

Based on the rapid diffusibility of CO_2, it was assumed that intracellular pCO_2 (pCO_{2c}), was given by,

$$pCO_{2c} = \frac{A_l \cdot pCO_{2l} + A_{bl} \cdot pCO_{2bl}}{A_l + A_{bl}} \tag{9}$$

Table 3. Values of the membrane parameters used in the model

	Luminal	Basolateral	Paracellular
A (cm^2)	1.0	14.3	0.01
L_p (cm/sec/atm)	1.0×10^{-5}	1.0×10^{-5}	0
w_i (cm/sec)			
Na^+	0	8.0×10^{-12}	1.4×10^{-7}
K^+	0	1.1×10^{-10}	1.4×10^{-7}
Cl^-	8.0×10^{-11}	0	0
HCO_3^-	0	0	0
H^+	0	0	0
σ^i			
Na^+	1.0	1.0	1.0
K^+	1.0	1.0	1.0
Cl^-	1.0	1.0	1.0
HCO_3^-	1.0	1.0	1.0
H^+	1.0	1.0	1.0

The permeabilities (L_p, w_i) are values per 1 cm^2 membrane.

where A_l and A_{bl} are the luminal and basolateral cell membrane areas, respectively. Values of A_l and A_{bl} are shown in Table 3.

2. Intrinsic Non-CO_2 Buffering System. For the intrinsic buffering system a weak base (B^-), was assumed to react with H^+ to produce its conjugate weak acid (HB),

$$H^+ + B^- \leftrightarrow HB \tag{10}$$

This equilibrium is governed by the law of mass action,

$$[H^+]_c[B^-]_c = K_{HB} \cdot [HB]_c \tag{11}$$

where K_{HB} is the apparent acid dissociation constant of the intrinsic non-CO_2 buffering system. The values of K_{HB} and the total intrinsic buffer ($[HB] + [B^-]$), B_{total}, were set at 0.04 mM and 6 M, respectively. These values were taken from experiments on pancreatic ducts in which an NH_4Cl prepulse was used to acid load the cells [40]. Figure 3 shows the pH-dependency of the intrinsic buffering capacity, β_c, of the model and is very similar to the experimental data [40]. The value of β_c used in the models corresponds to the buffering capacity at the midpoint of the $\triangle pH_c$ induced by an acid loading of 4–30 mM [40].

Fluid Compositions

The compositions of the bath solutions used in the models are given in Table 1. For most of the simulations we used either a HCO_3^-/CO_2-buffered solution or a HCO_3^-/CO_2-free, HEPES-buffered solution as indicated in the legends. The composition of these solutions was chosen to mimic those used by Novak & Greger in their experiments on microperfused pancreatic ducts [23, 24, 25]. To simulate the effects of increasing extracellular $[K^+]$, basolateral Na^+ was replaced by K^+. To simulate either Na^+-free or Cl^--free conditions these ions were replaced by an impermeable solute, X.

NUMERICAL SOLUTION

Figure 4 shows the sequence in which the model variables were computed. Given any set of model variables at time *t*, the program first calculated a temporary set of variables at time $t + dt$ from the transport equations (15*a*)–(15*d*) using Euler's method. Finally, a new set of model variables is obtained by modifying pH_c, $[HCO_3^-]_c$, $[HB]$ and

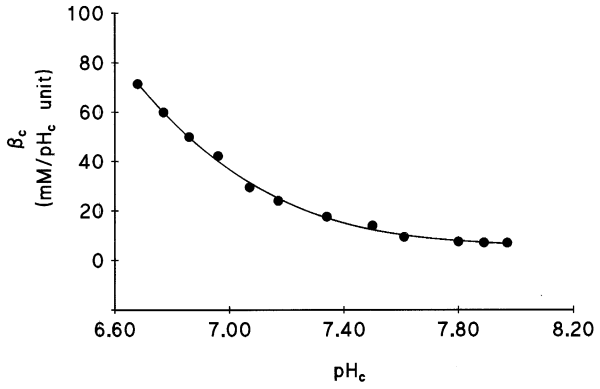

Fig. 3. pH-dependence of the intrinsic buffering capacity (β_c), of the computer model. The data points indicate the calculated buffering capacities at the midpoints of the pH_c change induced by acid loadings of 4–30 mM to the intrinsic buffering system of the model. The line was fitted by 3rd-order polynomial least squares regression analysis.

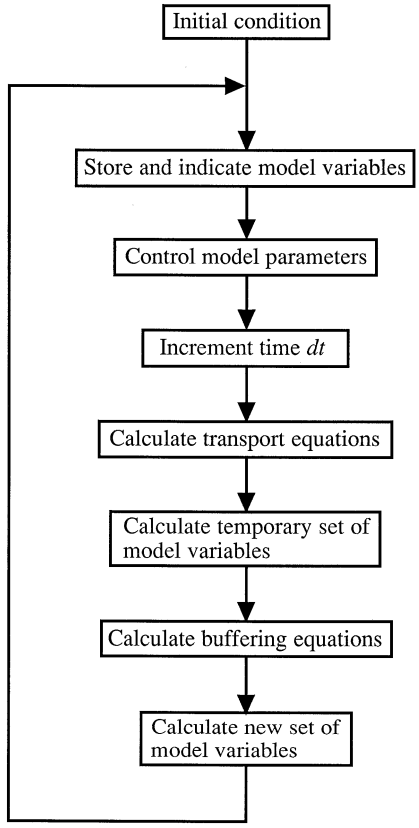

Fig. 4. Flow diagram showing the procedure for computing the model variables.

$[B^-]$ of the temporary variables according to the buffering equations (8) and (11).

Transport Equations

The fluxes of solute *i* across a membrane *m* ($J_{i(m)}$), for the basic model in which a basolateral Na^+ conductance was present, are given below,

$$J_{Cl(l)} = J_{dCl(l)} - J_{Cl/HCO3} \quad (12a)$$
$$J_{HCO3(1)} = J_{Cl/HCO3} \quad (12b)$$
$$J_{Na(bl)} = -3J_{pump} + J_{Na/H} + J_{dNa(bl)} \quad (12c)$$
$$J_{K(bl)} = 2J_{pump} + J_{dK(bl)} \quad (12d)$$
$$J_{H(bl)} = -J_{Na/H} \quad (12e)$$
$$J_{Na(j)} = J_{dNa(j)} \quad (12f)$$
$$J_{K(j)} = J_{dK(j)} \quad (12g)$$

For combinations of i and m other than those described above,

$$J_{i(m)} = 0 \quad (12h)$$

where positive flux is defined as solute movement in the basolateral to lumen direction.

The total fluxes of water and solute out of the intracellular compartment, $Flw_{v(c)}$ and $Flw_{i(c)}$ respectively, were described as,

$$Flw_{v(c)} = -J_{v(l)} + J_{v(bl)} \quad (13a)$$
$$Flw_{Na(c)} = J_{Na(bl)} \quad (13b)$$
$$Flw_{K(c)} = J_{K(bl)} \quad (13c)$$
$$Flw_{Cl(c)} = -J_{Cl(l)} + J_{Cl(bl)} \quad (13d)$$
$$Flw_{HCO3(c)} = -J_{HCO3(l)} \quad (13e)$$
$$Flw_{H(c)} = J_{H(bl)} \quad (13f)$$

A positive value indicates net influx into the intracellular compartment. The total fluxes of water and solutes into and out of the luminal and basolateral compartments were calculated in the same way.

The total electrical charge movement into compartment k, ($Flw_{e(k)}$), is described as,

$$Flw_{e(k)} = \sum_i z_i \cdot F \cdot Flw_{i(k)} \quad (14)$$

where positive current is defined as influx of positive charge into the compartment.

The model variables at time $t + dt$ before significant buffering had taken place, $Vol_{c,t+dt}$, $p_{(c),t+dt}$, $[i]_{c,t+dt}$ and $E_{(k),t+dt}$, were calculated from the transport equations (15a–15d) using Euler's method.

$$Vol_{k,t+dt} = Vol_{k,t} + Flw_{v(k)} \cdot dt \quad (15a)$$
$$p_{(k),t+dt} = p_{(k),t} + Flw_{v(k)} \cdot dt/C_{p(k)} \quad (15b)$$
$$[i]_{k,t+dt} = ([i]_{k,t} \cdot Vol_{k,t} + Flw_{i(c)} \cdot dt)/Vol_{k,t+dt} \quad (15c)$$
$$E_{(k),t+dt} = E_{(k),t} + Flw_{e(k)} \cdot dt/C_{e(k)} \quad (15d)$$

where dt is the integration interval; $C_{p(c)}$ is the compliance of the intracellular compartment; and $C_{e(k)}$ is the electrical capacitance of compartment k.

Membrane potentials were calculated using equation (15d). Using reasonable values for the integration interval (dt), and the electrical capacitance (C_e), this method can accurately determine transient changes in membrane potential. With values of dt = 20 msec and C_e = 8×10^{-4} Farads, the change in anion-cation gap in the cell remained within 0.006% of the control value throughout all simulations.

In equation (15b), the cell compliance ($C_{p(c)}$), was set to a large value (10^{80}) (*see* Table 2) because the static pressure difference between inside and outside of the cell was assumed to be negligible. During simulations, changes in the volumes, solute concentrations and static pressures of the luminal and basolateral compartments were negligible because the volumes and compliances of these compartments were all set to large values (*see* Table 2).

Of the model variables at time $t + dt$, those concerned with the buffering systems, $[H^+]_{c,t+dt}$, $[HCO_3^-]_{c,t+dt}$, $[B]_{c,t+dt}$ and $[HB]_{c,t+dt}$ were sequentially modified by the buffering equations. The other variables were not changed by buffering.

Buffering Equations

From Fig. 4, it can be seen that the buffering equations were calculated after the transport equations. Based on the rapidity of chemical reactions involved in the buffering process compared with transport phenomena, it was assumed that the buffering reactions were started and completed instantaneously at the end of the dt interval (at time $t + dt$).

Assuming that the unequilibrated buffering reactions shown in equations 7 and 10 were equilibrated by progressing to the right by x and y respectively:

$$[H^+] + [HCO_3^-] \xrightarrow{x} CO_2 + H_2O \quad (7')$$
$$[H^+] + [B^-] \xrightarrow{y} [HB] \quad (10')$$

then $[H^+]$ after equilibrium will given by $[H^+]-x-y$ because H^+ is dissipated by both the reactions shown in (7′) and (10′). $[HCO_3^-]$, $[B^-]$ and [HB] after equilibrium are given by $[HCO_3^-]-x$, $[B^-]-y$ and $[HB]+y$, respectively.

Therefore, from the buffering equations (8) and (11):

$$([H^+]'_{c-x-y})([HCO_3^-]'_{c-x}) = K_{CO2}\, pCO_{2c} \quad (16a)$$
$$([H^+]'_{c-x-y})([B^-]'_{c-y}) = K_{HB}([HB]'_{c+y}) \quad (16b)$$

where $[H^+]'_c$, $[HCO_3^-]'_c$, $[B^-]'_c$ and $[HB]'_c$ were intracellular concentrations of H^+, HCO_3^-, B^- and HB respectively at time $t + dt$ before equilibrium. The x and y parameters represent deviations from the equilibrium status in the HCO_3^-/CO_2 and intrinsic non-HCO_3^-/CO_2 buffering systems respectively. Values of x and y were derived from the simultaneous equations (16a) and (16b), and the buffered variables at time $t + dt$. $[H^+]_{c,t+dt}$, $[HCO_3^-]_{c,t+dt}$, $[B^-]_{c,t+dt}$ and $[HB]_{c,t+dt}$, were calculated as below:

$$[H^+]_{c,t+dt} = [H^+]'_{c-x-y} \quad (17a)$$
$$[HCO_3^-]_{c,t+dt} = [HCO_3^-]'_{c-x} \quad (17b)$$
$$[B^-]_{c,t+dt} = [B^-]'_{c-y} \quad (17c)$$
$$[HB]_{c,t+dt} = [HB]'_{c+y} \quad (17d)$$

Simulating Experimental Data

To simulate experimental data obtained under various conditions, the model parameters, for example, $[i]_{(bl)}$, w_i, $G_{Na/H}$ and $G_{Cl/HCO3}$, etc., were changed appropriately. The intact duct version of the model was usually run under open-circuit conditions. However, when the transepithelial potential difference (PD_{te}), was set to 0 mV, the short-circuit current (I_{sc}, defined as current flow from the basolateral to the luminal compartment) was given by,

$$I_{sc} = (Flw_{e(bl)}/C_{e(bl)} - Flw_{e(l)}/C_{e(l)})/(1/C_{e(bl)} + 1/C_{e(l)}) \quad (18)$$

The voltage divider ratio (VDR) was calculated using the following equation:

$$VDR = \left[\sum_i w_{i(bl)}\, \bar{c}_i\, z_i^2\, F^2) + G_{pump}\{[Na^+]_c/([Na^+]_c + K_{pNa})\}^3 \{[K^+]_{bl}/([K^+]_{bl} + K_{pK})\}^2\right] \Big/ \sum_i w_{i(l)}\, \bar{c}_i\, z_i^2\, F^2 \quad (19)$$

The conductance of the Na^+/K^+ pump is included into the basolateral conductance because the net charge flux by the Na^+/K^+ pump is dependent on PD_{bl}. However, its contribution to the total basolateral conductance is small.

Table 4. Parameter values used in the model for the Na^+/K^+ pump, the Na^+/H^+ antiporter and the Cl^-/HCO_3^- antiporter

Na^+/K^+ pump	
G_{pump} (mol/V/sec/cm^2)	4.38×10^{-8}
E_{rev} *(mV)*	−200
K_{pNa} (mM)	25
K_{pK} (mM)	1.4
Na^+/H^+ antiporter	
$G_{Na/H}$ (mol/sec/cm^2)	5×10^{-10}
K_{Na} (mM)	100
K_H (mM)	5×10^{-4}
Cl^-/HCO_3^- antiporter	
$G_{Cl/HCO3}$ (mol/sec/cm^2)	1.5×10^{-8}
K_{Cl} (mM)	10
K_{HCO3} (mM)	1

The permeabilities (G_{pump}, $G_{Na/H}$, $G_{Cl/HCO3}$) are values per 1 cm^2 membrane.

Parameter Selection

Values for the membrane and transport parameters that we employed are given in Tables 3 and 4 respectively. Using morphological data from a study on isolated rat pancreatic ducts [2], apical, basolateral and paracellular membrane areas were calculated to be 1.0, 14.3 and 0.01 cm^2/cm^2 epithelium respectively, and the cell volume to be 1.0 μl/cm^2 epithelium. Water permeabilities (L*p*), of the apical and basolateral membranes were set at 10^{-5} cm/sec/atm [34, 35, 36]. Lp of the paracellular pathway was assumed to be 0 cm/sec/atm. The resting permeability of the luminal membrane to Cl^- ($w_{Cl(l)} = 8 \times 10^{-11}$ cm/sec), and of the basolateral membrane to K^+ ($w_{K(bl)} = 1.1 \times 10^{-10}$ cm/sec) were calculated from measurements of the voltage divider ratio (VDR), in microperfused ducts [23, 24, 25]. We found that inclusion of a basolateral Na^+ conductance ($w_{Na(bl)}$) into the model was necessary to obtain accurate simulations of some experimental results.

Computer Calculations

The computer programs were written in FORTRAN and ran under the MS-DOS operating system on an IBM 386 PC compatible computer fitted with a maths coprocessor. The variables and constants in the programs were of the double precision data type. With $dt = 20$ msec., computation time was approximately one twentieth of the experimental time. Decreasing *dt* 10-fold had no effect on the calculated time courses of the model variables.

Results and Discussion

Steady-State Characteristics of the Model

The model remained in a steady state under each simulated condition when the membrane and transport parameters shown in Tables 3 and 4 were used. Steady-state values for the variables in the intact duct and the single-cell versions of the model are shown in Tables 5 and 6 respectively. Steady-state fluxes and turnover rates under each condition are given in Table 7.

Several of the steady-state model variables compare well with values reported in the literature. For instance, Table 5 shows that in the intact duct model, bathed with symmetrical CO_2/HCO_3^--free solutions, the basolateral membrane potential (PD_{bl}), the transepithelial potential (PD_{te}), the voltage divider ratio (VDR), the transepithelial resistance (R_{te}), and the equivalent short-circuit current (I_{sc}) were all similar to the values measured in microperfused ducts [23, 24, 25]. Moreover, for both the intact duct and the single-cell versions of the model, intracellular pH (pH_c), was about 7.2 when the cells were bathed in a CO_2/HCO_3^--buffered solution, which is similar to the measured value in the duct cell [38] (Tables 5 and 6). Tables 5 and 6 also show that on switching from a CO_2/HCO_3^--buffered solution to a HEPES-buffered solution, pH_c alkalinized by about 0.2 pH units which is consistent with experimental findings [38], (M.G. Raeder, *personal communication*). These quantitative similarities between computed and experimental data suggest

Table 5. Intact pancreatic duct model

	HEPES	HCO_3^-/CO_2	Experimental data (HEPES)
$[Na^+]_c$ (mM)	30.5	33.2	N/A
$[K^+]_c$ (mM)	100.4	105.0	N/A
$[Cl^-]_c$ (mM)	43.9	65.3	N/A
$[HCO_3^-]_c$ (mM)	0.2	16.1	N/A
pH_c	7.41	7.21	N/A
$[X]_c$ (mM)	140.4	95.8	N/A
Vol_{cell} (μl/cm^2)	1.00	1.28	~1
PD_{bl} (mV)	−65.2	−65.1	−63
PD_{te} (mV)	−1.0	−1.6	−0.8
VDR	8.4	8.2	8.2
R_{te} (Ωcm^2)	50	49.9	88
I_{sc} (μA/cm^2)	20.1	31.8	26

Steady state model variables for ducts bathed on both the luminal and basolateral sides with either a HCO_3^-/CO_2-free, HEPES-buffered, solution or a HCO_3^-/CO_2-buffered solution. Experimental data are taken from ref. 23. N/A = data not available.

Table 6. Isolated duct cell model

	HEPES	HCO_3^-/CO_2	Experimental data (HCO_3^-/CO_2)
$[Na^+]_c$ (mM)	30.5	33.3	N/A
$[K^+]_c$ (mM)	100.1	104.6	N/A
$[Cl^-]_c$ (mM)	43.2	64.3	N/A
$[HCO_3^-]_c$ (mM)	0.2	15.9	N/A
pH_c	7.41	7.20	7.18
$[X]_c$ (mM)	141.4	97.5	N/A
Vol_{cell} (μl/cm^2)	1.00	1.27	~1
PD (mV)	−65.0	−64.9	N/A

Steady-state model variables for single cells bathed in either a HCO_3^-/CO_2-free, HEPES-buffered, solution or a HCO_3^-/CO_2-buffered solution. Experimental data taken from ref. 38. N/A = data not available.

Table 7. Intact pancreatic duct model

Solution	HEPES	HCO_3^-/CO_2	
$w_{Cl(l)}$*	×1	×1	×20
$J_{dCl(l)}$	12.4	19.4	37.4
$J_{dNa(bl)}$	51.6	52.1	46.2
$J_{dK\ (bl)}$	−42.6	−47.7	−55.8
$J_{Na/H}$	12.4	19.4	37.4
J_{Cl/HCO_3}	12.4	19.4	37.4
J_{pump}	21.3	23.8	27.9

Steady-state ions fluxes and transporter turnover-rates (nmol/min/cm^2) in ducts on both the luminal and basolateral sides with either a HCO_3^-/CO_2-free, HEPES-buffered, solution or a HCO_3^-/CO_2-buffered solution. To mimic the effects of stimulation in the HCO_3^-/CO_2-buffered solution. the apical Cl^- conductance ($w_{Cl(l)}$) was increased 20-fold (* fold-change).

that our model accurately mimics the duct cell—at least in the steady state.

To date, no experimental data are available regarding the intracellular concentrations of Na^+, K^+ and Cl^- in pancreatic duct cells. The computer model predicts steady-state intracellular Na^+ and K^+ concentrations similar to those previously reported for other epithelial and nonepithelial cell types (Tables 5 and 6). In contrast, the steady-state intracellular Cl^- concentration ($[Cl^-]_c$) in a HCO_3^--containing medium (65 mM, *see* Tables 5 and 6) is somewhat higher than the value previously reported for other anion secreting epithelia (e.g., about 43 mM in nasal epithelium [44] and mandibular gland acinar cells [21]). However, the computer model predicts that $[Cl^-]_c$ falls sharply to values between 20 and 40 mM when stimulation is mimicked by increasing the apical membrane Cl^- conductance (Fig. 7*B*). A fall in $[Cl^-]_c$ following stimulation also occurs in mandibular gland acinar cells [21].

Effects of Basolateral K^+ Concentration and K^+ Conductance on Basolateral Membrane Potential

When microperfused rat pancreatic ducts are bathed in a CO_2/HCO_3^--free, HEPES-buffered, solution an increase in the basolateral K^+ concentration from 5 mM to 20 mM depolarizes PD_{bl} by 20 mV (from −61 to −41 mV), while basolateral application of 5 mM Ba^{2+} depolarizes PD_{bl} by 41 mV (from −64 to −23 mV) [25]. Figure 5(*A*) shows the computed time course of the changes in VDR and PD_{bl} following an increase in $[K^+]_{bl}$ and a decrease in $w_{K(bl)}$ in our computer model of an intact duct. Increasing $[K^+]_{bl}$ from 5 to 20 mM rapidly depolarized PD_{bl} by 23.4 mV (from −65.2 mV to −41.8 mV), and at the same time increased VDR. Both the depolarization and the change in VDR reversed immediately after $[K^+]_{bl}$ was returned to the control value.

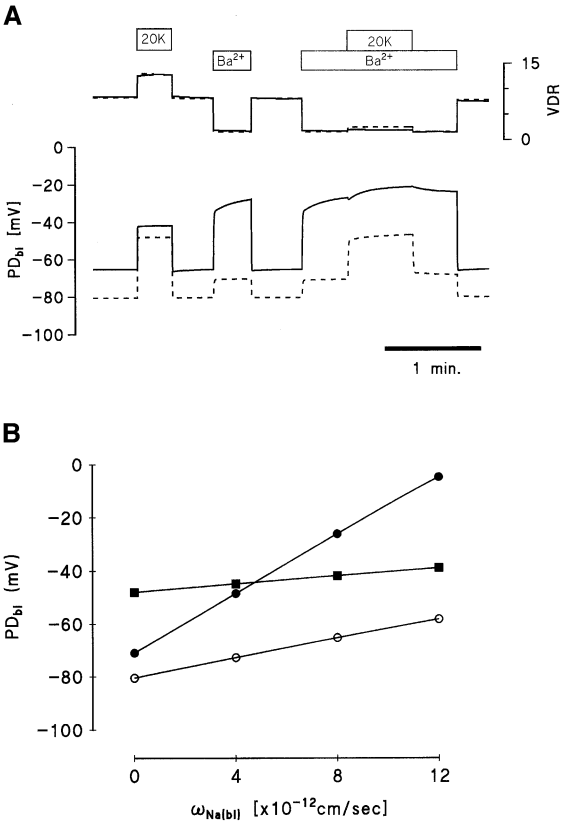

Fig. 5. Computer simulation of an intact pancreatic duct bathed with symmetrical HCO_3^-/CO_2-free, HEPES-buffered solutions. (*A*) Effect of changing the basolateral K^+ concentration ($[K^+]_{bl}$) and the basolateral membrane K^+ conductance ($w_{K(bl)}$) on the voltage divider ratio (VDR) and the basolateral membrane potential (PD_{bl}). These simulations were run with and without a basolateral Na^+ conductance ($w_{Na(bl)}$). Solid line: $w_{Na(bl)} = 8.0 \times 10^{-12}$ cm/sec, dashed line: $w_{Na(bl)} = 0$ cm/sec. $[K^+]_{bl}$ was increased by replacing Na^+ with K^+. (*B*) Relationship between PD_{bl} and $w_{Na(bl)}$. (○) PD_{bl} in control conditions, (■) PD_{bl} with $[K^+]_{bl} = 20$ mM, and (●) PD_{bl} with $w_{K(bl)} = 1.1 \times 10^{-11}$ cm/sec.

We mimicked the effect of basolateral Ba^{2+} by decreasing $w_{K(bl)}$ from 1.1×10^{-10} to 1.1×10^{-11} cm/sec. This reduced $w_{K(bl)}$ was calculated from the experimental value of the VDR (≈1.6) following addition of Ba^{2+} to isolated perfused pancreatic ducts [25]. It can be seen from Fig. 5*A* that reducing $w_{K(bl)}$ depolarized PD_{bl} by 37.2 mV (from −65.2 to −28.0 mV), and decreased VDR to about 1.6. Note that after $w_{K(bl)}$ had been decreased, raising $[K^+]_{bl}$ from 5 mM to 20 mM depolarized PD_{bl} by only 6 mV.

The time course, and the magnitude, of these computed changes in PD_{bl} and VDR following elevation of $[K^+]_{bl}$ and a reduction of $w_{K(bl)}$ are all very similar to the experimental data reported for microperfused rat ducts [23, 25]. However, changes in PD_{bl} that were consistent with the experimental data could only be produced by the model if a sodium conductance ($w_{Na(bl)}$), was included in the basolateral membrane.

Basolateral Na^+ Conductance

Figure 5*A* confirms that the presence of a $w_{Na(bl)}$ depolarizes PD_{bl}, and also affects the magnitude of the depolarizations caused by elevating $[K^+]_{bl}$ and reducing $w_{K(bl)}$. Moreover, the time courses of the PD_{bl} responses following elevation of $[K^+]_{bl}$ and a reduction in $w_{K(bl)}$ were slightly different when a basolateral Na^+ conductance was present in that a secondary, slow depolarization was observed (Fig. 5*A*). This slow depolarization can be explained by the fact that in the absence of a basolateral Na^+ conductance, PD_{bl} will be mainly determined by the K^+ gradient across the basolateral membrane. Therefore, when either $[K^+]_{bl}$ or w_{Kbl} is changed under these conditions, PD_{bl} will stay approximately constant. In contrast, when a Na^+ conductance is present on the basolateral membrane, PD_{bl} will be determined by both the K^+ and Na^+ gradients. A rapid depolarization of PD_{bl}, caused by a change in $[K]_{bl}$ or w_{Kbl}, will activate the Na^+/K^+ pump (it is voltage-dependent), decreasing $[Na^+]_c$ and thus increasing the Na^+ gradient across the basolateral membrane. The increased Na^+ gradient drives Na^+ influx which generates the slower depolarizations seen in Fig. 5*A*.

The relationship between the basolateral potential difference (PD_{bl}) and the basolateral Na^+ conductance ($w_{Na(bl)}$), under control conditions, in the presence of 20 mM extracelllar K^+, and with a reduced basolateral K^+ conductance is shown in Fig. 5*B*. As expected, it can be seen from the control plot (open circles) that as $w_{Na(bl)}$ alone is increased PD_{bl} depolarizes. Moreover, increasing $w_{Na(bl)}$ also affects the additional depolarization caused by elevating $[K^+]_{bl}$ (filled squares), and decreasing $w_{K(bl)}$ (filled circles). Note that the depolarizing effect of a reduced $w_{K(bl)}$ is enhanced as the Na^+ conductance increases (difference between the open and closed circle plots in Fig. 5*B*), but the reverse is true for the depolarization induced by high extracellular $[K^+]$ (difference between the open circle and close square plots in Fig. 5*B*). These effects can be clearly seen in the simulation shown in Fig. 5*A*. That the depolarization caused by a reduced $w_{K(bl)}$ is enhanced as the Na^+ conductance increases is best explained by assuming that PD_{bl} will not be effectively clamped at the K^+ equilibrium potential under these conditions. In contrast, the reduced effect of high $[K^+]_{bl}$ on PD_{bl} in the presence of a Na^+ conductance is probably explained by a fall in the electrochemical gradient driving Na^+ entry under these conditions. For microperfused ducts, Novak & Greger [23] reported that PD_{bl} in control cells, with $[K^+]_{bl} = 20$ mM and with 5 mM basolateral Ba^{2+} were −63, −41 and −32 mV respectively. From Fig. 5 it can be seen that the value of $w_{Na(bl)}$ which could best explain these experimental data is about 8.0×10^{-12} cm/sec, and so this level of Na^+ conductance was included in the model for all other simulations.

It was reported by Novak & Greger [23] that there was no significant Na^+ diffusive pathway on the basolateral membrane of rat pancreatic duct cells. However, setting $w_{Na(bl)}$ in the computer model to 8.0×10^{-12} cm/sec (equivalent to only 7% of $w_{K(bl)}$), and assuming that the paracellular pathway conducts choline as effectively as Na^+ and K^+, we found that reducing $[Na^+]_{bl}$ to 0.1 mM by replacement with choline only hyperpolarized PD_{bl} by about 14 mV (*data not shown*). Thus the model predicts that a large fall in $[Na^+]_{bl}$ has only a relatively small hyperpolarizing effect on PD_{bl}. Such a small hyperpolarization would be difficult to detect experimentally if, as seems likely, removal of extracellular Na^+ also acidifies the cell (via inhibition of the Na^+/H^+ exchangers) and inhibits the basolateral K^+ conductance [23].

A number of transport pathways have been described in the duct cell which could produce the basolateral Na^+ conductance predicted by the computer model. Gray et al. [8] reported the presence of nonselective cation channels on rat pancreatic duct cells. However, these channels were observed in only 1 out of 1027 cell-attached patches on unstimulated duct cells indicating that their activity is very low [8]. A second possibility is that the Na^+ conductance is linked to Ca^{2+} movements. Based on the finding that extracellular Ca^{2+} removal causes a rapid fall in intracellular Ca^{2+} concentration, Stuenkel & Hootman [37] and Ashton et al. [4] concluded that pancreatic duct cells have a relatively large resting Ca^{2+} permeability. Although they have yet to be identified on the duct cell, the combination of a Ca^{2+} channel and an electrogenic Na^+/Ca^{2+} antiporter could, in theory, depolarize the basolateral membrane. At steady state, Ca^{2+} influx via the channels should be balanced by Ca^{2+} efflux on the antiporter. Thus the charge movement carried by Na^+ influx on the electrogenic antiporter could generate the basolateral Na^+ conductance predicted by our computer model. However, it should be noted that the influx of Na^+ would lead to the electrogenic extrusion of Na^+ through the Na^+-K^+ pump and to the release of K^+ through potassium channels, both of which would tend to nullify the steady-state depolarization. Finally, a Na^+-$(HCO_3^-)_n$ cotransporter has recently been identified on the basolateral membrane of rat [47], pig [42], and guinea-pig duct cells [17]. The stoichiometry of this transporter has not been established; however, unlike the Na^+-$(HCO_3^-)_3$ symport described in the kidney [27], it would have to carry a net positive charge to depolarize the duct cell.

Effects of Extracellular Na^+ Concentration and Permeability of the Na^+/H^+ Antiporter on Intracellular pH

The basolateral membrane of rat and guinea-pig pancreatic duct cells contains a Na^+/H^+ antiporter [23, 38] (Fig.

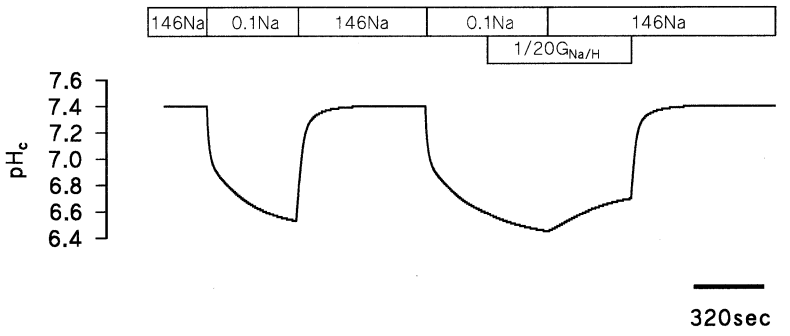

Fig. 6. Computer simulation of an isolated pancreatic duct cell bathed in HCO_3^-/CO_2-free, HEPES-buffered, solution. The effect of reducing the extracellular Na^+ concentration ($[Na^+]_b$), and the activity of the Na^+/H^+ exchanger ($G_{Na/H}$), on intracellular pH (pH_c). Na^+ was replaced by an impermeant cation.

1). Figure 6 shows how changes in extracellular Na^+ concentration ($[Na^+]_b$), and in the permeability coefficient of the Na^+/H^+ antiporter ($G_{Na/H}$), affect intracellular pH (pH_c) in our computer model. This simulation was performed using the single-cell version of the model bathed with a HCO_3^-/CO_2-free, HEPES-buffered solution. Decreasing $[Na^+]_b$ from 146 to 0.1 mM acidified the cell from pH 7.40 to pH 6.53, and this effect was fully reversed on replacement of extracellular Na^+ (Fig. 6). A decrease in $G_{Na/H}$ from 5×10^{-10} to 2.5×10^{-11} cm/sec did not change the value of pH_c at the acidified plateau, but did block the recovery from acidification following re-introduction of $[Na^+]_b$ (Fig. 6). The time course of these changes of pH_c in our computer model are very similar to experimental data reported by Stuenkel et al. [38] for the effects of $[Na^+]_b$ removal and amiloride (reduced $G_{Na/H}$) on duct cell pH_c.

Effects of Extracellular Cl^- Concentration and Permeability of the Cl^-/HCO_3^- Antiporter on Intracellular pH

The apical membrane of the duct cell contains an electroneutral Cl^-/HCO_3^- antiporter [24] together with Cl^- channels [9, 11, 24, 38] (Fig. 1). Figure 7 shows how changes in extracellular Cl^- concentration ($[Cl^-]_b$), and in the permeability of the Cl^-/HCO_3^- antiporter ($G_{Cl/HCO3}$) affect pH_c in our computer model. This simulation was performed using the single-cell version of the model bathed with HCO_3^-/CO_2-buffered solution. Decreasing $[Cl^-]_b$ from 150 to 0.1 mM caused a rapid alkalinization of pH_c from pH 7.20 to pH 7.95, an effect that was fully reversed when extracellular $[Cl^-]_b$ was replaced (Fig. 7). Decreasing $G_{Cl/HCO3}$ from 1.5×10^{-8} to 7.5×10^{-10} cm/sec did not change pH_c at the plateau of the alkalinization, but did slow the recovery in pH_c following the return of $[Cl^-]_b$ (Fig. 7). The time course of the changes in pH_c produced by the model are very similar to the experimental data reported by Stuenkel et al. [38] for the effects of $[Cl^-]_b$ removal and DIDS on pH_c in isolated guinea-pig ducts.

Effects of Luminal Cl^- Conductance on HCO_3^- Secretion

Patch-clamp studies have shown that the luminal Cl^- conductance of pancreatic duct cells is mediated by cystic fibrosis transmembrane conductance regulator (CFTR) Cl^- channels [9, 11, 24], and Ca^{2+}-activated Cl^- channels [12, 45]. These Cl^- channels are key regulatory points in the HCO_3^- secretory mechanism because they allow recycling of Cl^- through the apical Cl^-/HCO_3^- exchanger [3].

Figure 8*A* shows the effect of altering luminal Cl^- permeability ($w_{Cl(l)}$), on HCO_3^- flux across the luminal membrane via the Cl^-/HCO_3^- antiporter ($J_{HCO3(l)}$), intracellular Cl^- concentration ($[Cl^-]_c$), intracellular pH (pH_c), the voltage-divider ratio (VDR) and the basolateral potential difference (PD_{bl}). For this simulation the luminal and basolateral membranes were bathed in the HCO_3^-/CO_2-buffered solution. Increasing $w_{Cl(l)}$ increased $J_{HCO3(l)}$, decreased $[Cl^-]_c$, acidified the cell, decreased the VDR and depolarized PD_{bl}. A 20-fold increase in $w_{Cl(l)}$, as occurs following maximal stimulation of the duct cell [11, 25] increased $J_{HCO3(l)}$ from 19.4 to 37.4 nmol/min/cm^2 (*see* Table 7). This 1.9-fold increase in $J_{HCO3(l)}$ is consistent with experimental results obtained from isolated rat pancreatic ducts using micropuncture techniques which show that maximal doses of either secretin or acetylcholine approximately double the basal rate of fluid secretion [4]. These computed data confirm that the luminal Cl^--conductance is one of the regulatory points for HCO_3^--secretion in pancreatic duct cells.

Figure 8*B* summarizes the relationship between $w_{Cl(l)}$ and $J_{HCO3(l)}$, and between $w_{Cl(l)}$ and the intracellular Cl^- concentration ($[Cl^-]_c$). Note that as $w_{Cl(l)}$ increases there are reciprocal changes in $[Cl^-]_c$ and $J_{HCO3(l)}$, with $J_{HCO3(l)}$ increasing and $[Cl^-]_c$ decreasing. These data confirm that in the unstimulated duct cell (when $w_{Cl(l)}/w_{Cl(l)\ control} = 1$), intracellular Cl^- concentration is quite high—somewhere between 40 and 70 mM depending on the basolateral K^+ conductance (Fig. 8*B*).

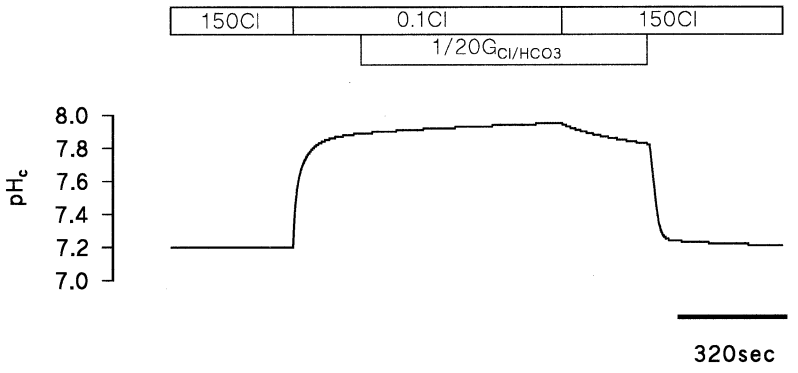

Fig. 7. Computer simulation of an isolated pancreatic duct cell bathed in a HCO_3^-/CO_2-buffered solution. Effect of reducing the extracellular Cl^- concentration ($[Cl^-]_b$), and the activity of the Cl^-/HCO_3^- exchanger on intracellular pH (pH_c). Cl^- was replaced by an impermeant anion.

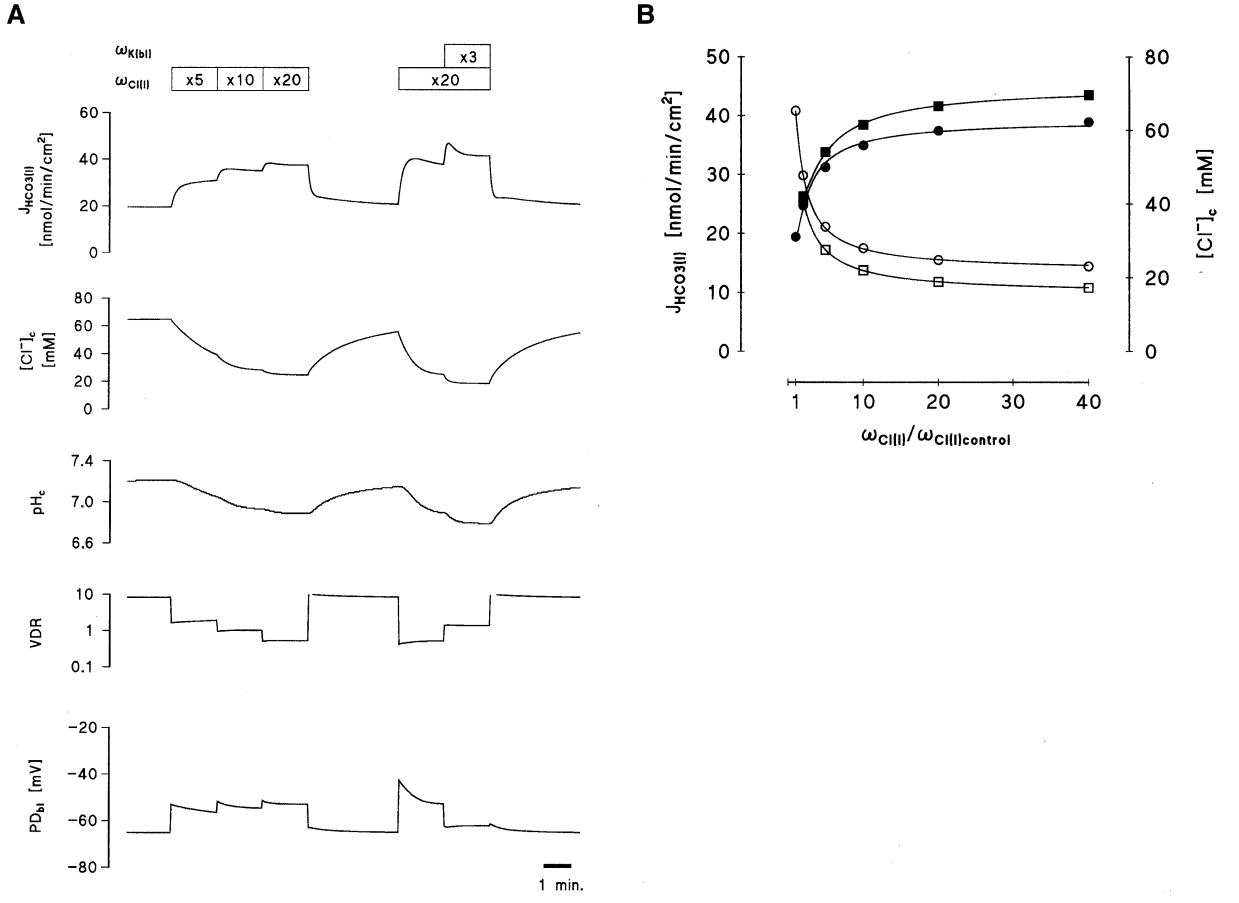

Fig. 8. Computer simulation of an intact pancreatic duct bathed with symmetrical HCO_3^-/CO_2-buffered solutions. (*A*) Effect of increasing the apical Cl^- conductance ($w_{Cl(l)}$), and the basolateral K^+ conductance ($w_{K(bl)}$) on HCO_3^- secretion ($J_{HCO3(1)}$), intracellular Cl^- concentration ($[Cl^-]_c$), intracellular pH (pH_c), the voltage divider ratio (VDR), and the basolateral membrane potential (PD_{bl}). (*B*) Summary of the effects of $w_{Cl(l)}$ on $J_{HCO3(l)}$ and $[Cl^-]_c$. Solid symbols, $J_{HCO3(l)}$. Open symbols, $[Cl^-]_c$. Circles, $w_{K(bl)} = 1.1 \times 10^{-10}$cm/sec (x1). Squares, $w_{K(bl)} = 3.3 \times 10^{-10}$ cm/sec (×3).

Effects of Basolateral K^+ Conductance on HCO_3^- Secretion

The next question we addressed was the relationship between the magnitude of the basolateral K^+ conductance and HCO_3^- secretion at the apical membrane of the duct cell. Clearly, the dominant conductance change following stimulation is an increase in the apical Cl^- conductance because the cells depolarize [24]. However, this does not rule out the possibility that some increase in

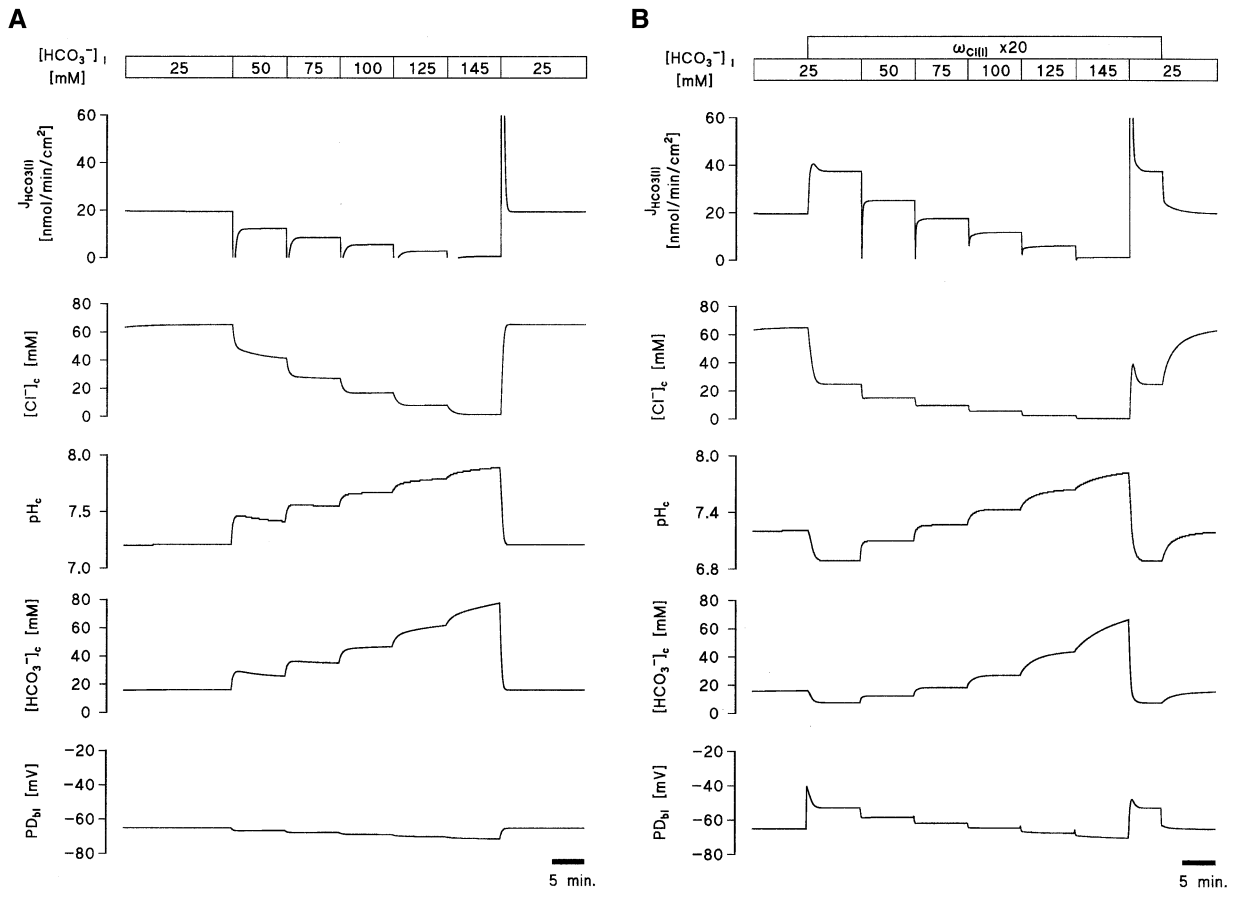

Fig. 9. Computer simulation of an intact pancreatic duct bathed in HCO_3^-/CO_2-buffered solutions. (*A* and *B*) Effect of increasing the luminal HCO_3^- concentration ($[HCO_3^-]_l$) on bicarbonate secretion ($J_{HCO3(l)}$), intracellular Cl^- concentration ($[Cl^-]_c$), intracellular HCO_3^- concentration ($[HCO_3^-]_c$), intracellular pH (pH_c), and the basolateral membrane potential (PD_{bl}). (*A*) Data from an unstimulated duct, $w_{Cl(l)} = 8 \times 10^{-11}$ cm/sec. (*B*) Data from a stimulated duct, $w_{Cl(l)} = 1.6 \times 10^{-9}$ cm/sec.

basolateral K^+ conductance also occurs. In fact, cAMP-activated, maxi-K^+, channels have been identified on the basolateral membrane of rat duct cells [10]. Figure 8*A* shows that a 3-fold increase in $w_{K(bl)}$ hyperpolarized PD_{bl} from about −53 to −62 mV, and increased $J_{HCO3(l)}$ by approximately 10%. Thus the computer model predicts that relatively small changes in $w_{K(bl)}$ can affect HCO_3^- secretion and, therefore, that the basolateral K^+ conductance should be considered as a potential regulatory site in the HCO_3^- secretory mechanism.

Effects of Luminal HCO_3^- Concentration on HCO_3^- Secretion

One key question is whether the computer model can secrete HCO_3^- at the concentrations found in pancreatic juice under physiological conditions. As mentioned above most of the experimental data on which the model is based has come from studies on the rat. In this species there is a relatively high rate of secretion from the unstimulated gland and this basal juice has a HCO_3^- concentration of about 25 mM. Following maximal stimulation with secretin there is an increase in juice flow rate and the HCO_3^- concentration rises to about 70 mM [30]. The situation is somewhat different in humans, cats, dogs and guinea pigs. In these species there is little or no secretion from the unstimulated gland; however, following exposure to secretin the volume of juice increases and the HCO_3^- concentration rises from about 50 mM at low flow rates up to 145 mM at the maximum flow rate [5]. This flow rate dependency of the HCO_3^- concentration in pancreatic juice results from a secondary, passive, anion exchange process (exchanging luminal HCO_3^- for blood Cl^-) that exists within the ductal system [3, 5]. It is generally assumed that the maximal HCO_3^- concentration in pancreatic juice (i.e., the concentration observed

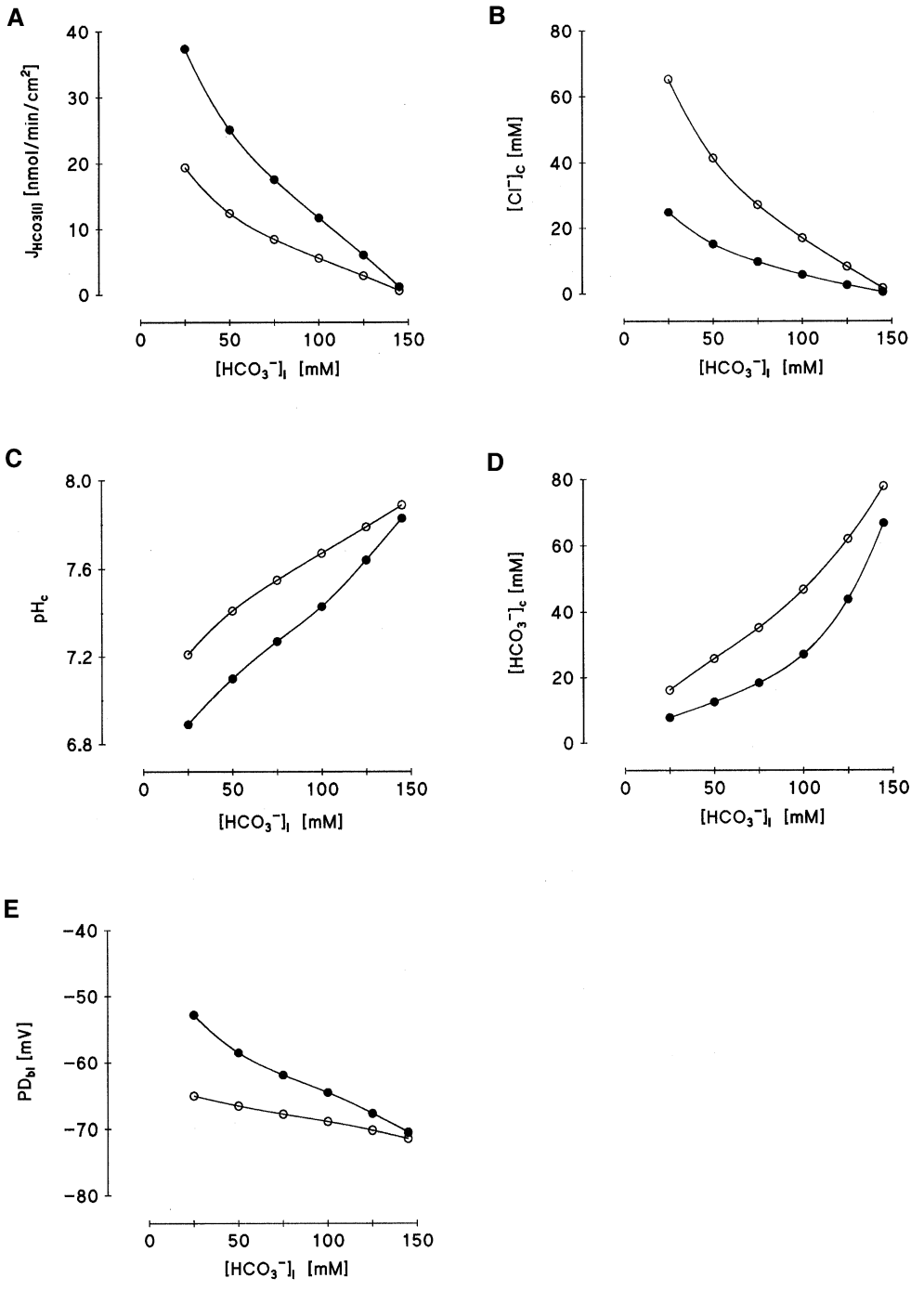

Fig. 10. Computer simulation of an intact pancreatic duct bathed in HCO_3^-/CO_2-buffered solutions. Relationship between luminal HCO_3^- concentration ($[HCO_3^-]_l$) and: (*A*) bicarbonate secretion ($J_{HCO3(l)}$), (*B*) intracellular Cl^- concentration ($[Cl^-]_c$), (*C*) intracellular pH (pH_c), (*D*) intracellular HCO_3^- concentration ($[HCO_3^-]_c$), and (*E*) basolateral membrane potential (PD_{bl}). Open symbols, unstimulated duct, $w_{Cl(l)} = 8 \times 10^{-11}$ cm/sec. Closed symbols, stimulated duct, $w_{Cl(l)} = 1.6 \times 10^{-9}$ cm/sec. Data were recorded 500 sec after a step change in $[HCO_3^-]_l$.

at the maximum flow rate when there is least time available for anion exchange) represents the composition of the primary fluid secreted by the duct cell. We investigated the model's ability to secrete bicarbonate simply by increasing the HCO_3^- concentration in the luminal compartment ($[HCO_3^-]_l$) and observing the effect on $J_{HCO3(1)}$, and on a number of other cellular parameters.

Figure 9*A* and *B* show the effect of luminal HCO_3^-

concentration ($[HCO_3^-]_l$) on $J_{HCO3(l)}$, $[Cl^-]_c$ and pH_c in unstimulated (Fig. 9*A*) and stimulated cells (Fig. 9*B*). Duct stimulation was mimicked by increasing the Cl^- conductance of the apical membrane by 20-fold. Initially, the standard HCO_3^-/CO_2-buffered solution ($[HCO_3^-]$ = 25 mM) was present on both the basolateral and the luminal sides of the epithelium. The luminal HCO_3^- concentration ($[HCO_3^-]_l$), was then increased in 25 mM steps to 145 mM by replacing Cl^- with HCO_3^-. Assuming pCO_2 remained constant at 40 mm Hg, this maneuver will alkalinize pH_l from 7.4 to 8.2. As can be seen from Fig. 9*A* and *B* sequentially increasing $[HCO_3^-]_l$ from 25 to 145 mM, without any other changes in the model parameters, markedly reduced $J_{HCO3(l)}$. At the same time there was a marked fall in $[Cl^-]_c$, a marked rise in pH_c and $[HCO_3^-]_c$, and a hyperpolarization of PD_{bl}.

Figure 10 is a detailed quantitative comparison of the data shown in Fig. 9*A* and *B.* Figure 10*A* shows that in both stimulated and unstimulated ducts, $J_{HCO3(l)}$ falls as the HCO_3^- concentration in the lumen increases. Note also that the increase in $J_{HCO3(l)}$ that occurs following stimulation (the difference between unstimulated and stimulated plots in Fig. 10*A*) also decreases as the luminal HCO_3^- rises. From Fig. 10*A–E* it is clear that the model cell shown in Fig. 1 will secrete HCO_3^- at around the maximum concentration found in rat pancreatic juice (75 mM). At this luminal HCO_3^- concentration there is a doubling of $J_{HCO3(l)}$ from 8.7 to 17.6 nmol/min/cm^2 following a 20-fold increase in $w_{Cl(l)}$ (Fig. 10*A*), which is consistent with experimental data obtained from isolated pancreatic ducts [4]. Moreover, the intracellular and electrical parameters are within the ranges expected for mammalian cells—pH_c falls from (7.55 to 7.27); $[Cl^-]_c$ falls from (21.7 to 9.8 mM); $[HCO_3^-]_c$ falls from (35.1 to 18.3 mM); and PD_{bl} depolarizes from −67.8 to −61.9 mV. However, it is also clear from Fig. 10*A–E* that the model will not produce pancreatic juice with a HCO_3^- concentration equivalent to that found in cats, guinea pigs, dogs and man (about 145 mM). As luminal HCO_3^- approaches 145 mM the cellular parameters move outside the ranges that would normally be expected for most cells under physiological conditions; e.g., intracellular Cl^- concentration is close to zero (Fig. 10*B*); intracellular pH is close to 8 (Fig. 10*C*); and intracellular HCO_3^- is about 80 mM (Fig. 10*D*). Moreover, PD_{bl} is about −75 mV in unstimulated ducts and is hardly affected by a 20-fold increase in $w_{Cl(l)}$ (Fig. 10*E*).

Conclusions and Predictions from the Mathematical Model

In conclusion, our mathematical model of the pancreatic duct cell, which is largely based on data obtained from the rat, accurately mimics many experimental findings in both the steady and nonsteady states. Moreover, the model makes a number of predictions that could be tested experimentally, e.g., (i) there is likely to be a Na^+ conductance pathway on the basolateral membrane of the duct cell, (ii) the resting $[Cl^-]_c$ of the duct cell is quite high (65.3 mM in a HCO_3^-/CO_2 solution), and falls sharply when the cells are stimulated, and (iii) intracellular pH falls when the cells are stimulated to secrete HCO_3^- ions. Finally, the computer simulation suggests that while the basic duct cell model as shown in Fig. 1 could produce pancreatic juice with a HCO_3^- concentration of about 75 mM as found in the rat, it cannot support secretion of HCO_3^- at the much higher concentrations (up to 145 mM) found in the pancreatic juice of cats, guinea pigs, dogs and man. To secrete almost isotonic $NaHCO_3$, while at the same time maintaining reasonable values for the intracellular ion concentrations and pH_c, the model will have to be modified.

Finally, in this paper we have focused our attention on the original HCO_3^- secretory model as proposed by Gray et al. [9] and Novak and Greger [24]. However, it is worth noting that since this model was proposed a number of other transport elements have been identified in the duct cell, including an H^+ ATPase [28], and a $Na(HCO_3^-)_n$ cotransporter [17, 42, 47]. We anticipate that future versions of our computer model will incorporate these additional transport elements.

Funded by the Cystic Fibrosis Trust and the Medical Research Council (UK).

References

1. Apell, H.J. 1989. Electrogenic properties of the Na,K pump. *J. Membrane Biol.* **110:**103–114
2. Argent, B.E., Arkle, S., Cullen, M.J., Green, R. 1986. Morphological, biochemical and secretory studies on rat pancreatic ducts maintained in tissue culture. *Q. J. Exp. Physiol.* **71:**633–648
3. Argent, B.E., Case, R.M., 1994. Pancreatic ducts. Cellular mechanism and control of bicarbonate secretion. *In:* Physiology of the Gastrointestinal Tract. (3rd Ed.) L.R. Johnson, editor. pp. 1473–1497. Raven Press, New York
4. Ashton, N., Evans, R.L., Elliott, A.C., Green, R., Argent, B.E. 1993. Regulation of fluid secretion and intracellular messengers in isolated rat pancreatic ducts by acetylcholine. *J. Physiol.* **471:**549–562
5. Case, R.M., Argent, B.E. 1993. Pancreatic duct cell secretion. Control and Mechanisms of Transport. *In:* The Pancreas: Biology, Pathobiology, and Disease. (2nd Ed.) V.L.W. Go, E.P. DiMagno, J.D. Gardner, E. Lebenthal, H.A. Reber and G. Scheele, editors. pp. 301–350. Raven Press, New York
6. Cook, D.I., Young, J.A. 1989. Effects of K^+ channels in the apical membrane on epithelial secretion based on secondary active Cl^- transport. *J. Membrane Biol.* **110:**139–146
7. Fernandes, P.L., Ferreira, H.G. 1991. A mathematical model of rabbit cortical thick ascending limb of the Henle's loop. *Biochim. Biophys. Acta.* **1064:**111–123
8. Gray, M.A., Argent, B.E. 1990. Non-selective cation channel on pancreatic duct cells. *Biochim. Biophys. Acta* **1029:**33–42

9. Gray, M.A., Greenwell, J.R., Argent, B.E. 1988. Secretin-regulated chloride channel on the apical membrane of pancreatic duct cells. *J. Membrane Biol.* **105:**131–142
10. Gray, M.A., Greenwell, J.R., Garton, A.J., Argent, B.E. 1990. Regulation of maxi-K^+ channels on pancreatic duct cells by cyclic AMP-dependent phosphorylation. *J. Membrane Biol.* **115:**203–215
11. Gray, M.A., Plant, S., Argent, B.E. 1993. cAMP-regulated whole cell chloride currents in pancreatic duct cells. *Am. J. Physiol.* **264:**C591–C602
12. Gray, M.A., Winpenny, J.P., Porteous, D.J., Dorin, J.R., Argent, B.E. 1994. CFTR and calcium-activated chloride currents in pancreatic duct cells of a transgenic CF mouse. *Am. J. Physiol.* **266:**C213–C221
13. Hartmann, T., Verkman, A.A. 1990. Model of ion transport regulation in chloride-secreting airway epithelial cells. *Biophys. J.* **58:**391–401
14. Hellmessen, W., Christian, A.L., Fasold, H., Schulz, I. 1985. Coupled Na^+-H^+ exchange in isolated acinar cells from rat exocrine pancreas. *Am. J. Physiol.* **249:**G125–G136
15. Hoffmann, E.K., Simonsen, L.O. 1989. Membrane mechanisms in volume and pH regulation in vertebrate cells. *Physiol. Rev.* **69:** 315–382
16. Imai, Y. 1989. Membrane transport system modelled by network thermodynamics. *J. Membrane Sci.* **41:**3–21
17. Ishiguro, H., Lindsay, A.R.G., Steward, M.C., Case, R.M. 1994. Regulation of intracellular pH in interlobular ducts isolated from guinea-pig pancreas. *J. Physiol.* **479.P:**10P
18. Kohn, O.F., Mitchell, P.P., Steinmetz, P.R. 1990. Characteristics of apical Cl-HCO_3 exchanger of bicarbonate-secreting cells in turtle bladder. *Am. J. Physiol.* **258:**F9–F14
19. Kuijpers, G.A.J., DePont, J.J.H.H.M., Westerhoff, H.V. 1989. A model for fluid secretion in the exocrine pancreas. *Biochim. Biophys. Acta* **948:**71–80
20. Larsen, E.H., Rasmussen, B.E. 1982. Chloride channels in toad skin. *Phil. Trans. R. Soc. Lond. B.* **299:**413–434
21. Lau, K.R., Case, R.M. 1988. Evidence for apical chloride channels in rabbit mandibular salivary clands. A chloride-selective microelectrode study. *Pfluegers Arch.* **411:**670–675
22. Lew, V.L., Ferreira, H.G., Moura, T. 1979. The behaviour of transporting epithelial cells. 1. Computer analysis of a basic model. *Proc. R. Soc. Lond. B.* **206:** 58–83
23. Novak, I., Greger, R. 1988. Electrophysiological study of transport systems in isolated perfused pancreatic ducts: properties of the basolateral membrane. *Pfluegers Arch.* **411:**58–68
24. Novak, I., Greger, R. 1988. Properties of the luminal membrane of isolated perfused rat pancreatic ducts: Effects of cyclic AMP and blockers of chloride transport. *Pfluegers Arch.* **411:**546–553
25. Novak, I., Greger, R. 1991. Effects of bicarbonate on potassium conductance of isolated perfused rat pancreatic ducts. *Pfluegers Arch.* **419:**76–83
26. Oster, G.F., Perelson, A.S., Katchalsky, A. 1973. Network thermodynamics: dynamic modelling of biophysical systems. *Quart. Rev. Biophys.* **6:**1–134
27. Preisig, P.A., Alpern, R.J. 1989. Basolateral membrane H-OH-HCO_3 transport in the proximal tubule. *Am. J. Physiol.* **256:**F751–F765
28. Raeder, M.G. 1992. The origin and subcellular mechanisms causing pancreatic bicarbonate secretion. *Gastroenterology* **103:**1674–1684
29. Rakowski, R.F. 1993. Charge movement by the Na/K pump in *Xenopus* oocytes. *J. Gen. Physiol.* **101:**117–144
30. Sewell, W.A., Young, J.A. 1975. Secretion of electrolytes by the pancreas of the anaesthetized rat. *J. Physiol.* **252:**379–396
31. Sjaastad, M.D., Wenzl, E., Machen, T.E. 1992. pH_i dependence of Na-H exchange and H delivery in IEC-6 cells. *Am. J. Physiol.* **262:**C164–C170
32. Sohma, Y., Argent, B.E., Gray, M.A., Imai, Y. 1993. Computer model of pancreatic duct cells. *J. Physiol.* **467:**243P
33. Sohma, Y., Gray, M.A., Imai, Y., Argent, B.E. 1995. Effects of apical Cl^- conductance on HCO_3^- secretion by a computer model of rat pancreatic duct cells. *J. Physiol.* **482.P:**31P
34. Spring, K.R. 1983. Fluid transport by gallbladder epithelium. *J. Exp. Biol.* **106:**181–194
35. Steward, M.C., Garson, M.J. 1985. Water permeability of *Necturus* gallbladder epithelial cell membranes measured by nuclear magnetic resonance. *J. Membrane Biol.* **86:**203–210
36. Strange, K., Spring, K.R. 1987. Cell membrane permeability of rabbit cortical collecting duct. *J. Membrane Biol.* **96:**27–43
37. Stuenkel, E.L., Hootman, S.R. 1990. Secretagogue effects on intracellular calcium in pancreatic duct cells. *Pfluegers Arch.* **416:**652–658
38. Stuenkel, E.L., Machen, T.E., Williams, J.A. 1988. pH regulatory mechanisms in rat pancreatic ductal cells. *Am. J. Physiol.* **254:** G925–G930
39. Toennessen, T.I., Sandvig, K., Olsenes, S. 1990. Role of Na^+-H^+ and Cl^-–HCO_3^- antiports in the regulation of cytosolic pH near neutrality. *Am. J. Physiol.* **258:**C1117–C1126
40. Veel, T., Villanger, O., Holthe, M.R., Cragoe, E.J. Jr., Raeder, M.G. 1990. Na^+–H^+ exchange is not important for pancreatic HCO_3^- secretion in the pig. *Acta Physiol. Scand.* **144:**239–246
41. Verkman, A.S., Alpern, R.J. 1987. Kinetic transport model for cellular regulation of pH and solute concentration in the renal proximal tubule. *Biophys. J.* **51:**533–546
42. Villanger, O., Veel, T., Raeder, M.R. 1995. Secretin causes H^+/HCO_3^- secretion from pig pancreatic ductules by vacuolar-type H^+-adenosine triphosphatase. *Gastroenterology* **108:**850–859
43. Weinstein, A. 1992. Chloride transport in a mathematical model of the rat proximal tubule. *Am. J. Physiol.* **263:**F860–F873
44. Willumsen, N.J., Davis, C.W., Boucher, R.C. 1989. Intracellular Cl^- activity and cellular Cl^- pathways in cultured human airway epithelium. *Am. J. Physiol.* **256:**C1033–C1044
45. Winpenny, J.P., Verdon, B., McAlroy, H., Colledge, W.H., Ratcliff, R., Evans, M.J., Gray, M.A., Argent, B.E. 1994. Calcium-activated chloride conductance is not increased in pancreatic duct cells of CF mice. *Pfluegers Arch.* **430:**26–33
46. Wu, M.M., Civan, M.M. 1991. Voltage dependence of current through the Na,K-exchange pump of Rana oocytes. *J. Membrane Biol.* **121:**23–36
47. Zhao, H., Star, R.A., Muallem, S. 1994. Membrane localisation of H^+ and HCO_3^- transporters in the rat pancreatic duct. *J. Gen. Physiol.* **104:**57–85